

Confinement sensitivity in quantum dot singlet-triplet relaxation

C. J. Wesslén¹ and E. Lindroth¹

¹*Department of Physics, Stockholm University, AlbaNova, S-106 91 Stockholm, Sweden*

(Dated: April 18, 2022)

Spin-orbit mediated phonon relaxation in a two-dimensional quantum dot is investigated using different confining potentials. Elliptical harmonic oscillator and cylindrical well results are compared to each other in the case of a two-electron GaAs quantum dot subjected to a tilted magnetic field. The lowest energy set of two-body singlet and triplet states are calculated including spin-orbit and magnetic effects. These are used to calculate the phonon induced transition rate from the excited triplet to the ground state singlet for magnetic fields up to where the states cross. The roll of the cubic Dresselhaus effect and the positioning of "spin hot-spots" are discussed and relaxation rates for a few different systems are exhibited.

PACS numbers:

I. INTRODUCTION

Quantum dots (QDs) created through semiconductor heterostructures are promising components in the fields of spintronics, quantum information and quantum computing^{1,2}. For time sensitive applications, as when operations are to be performed on excited electron states within their coherence time, a long relaxation time is a decisive property. Long lifetimes are expected if the decay requires a spin flip and experimental studies have here measured excited state relaxation on the microsecond to millisecond timescale³⁻⁶, with the longest life times for dots subjected to a magnetic field. It is important to understand, and to quantitatively model, the dominating electronic and spin-dependent relaxation processes.

The role of the magnetic field is to suppress direct spin exchange with bulk material nuclei⁴. The still occurring relaxation is in this situation believed to be dominated by phonon exchange, but this mechanism opens the route to spin flips only in combination with spin-orbit coupling. This has been an important area of study, both for single electron⁷⁻⁹ and multi electron states^{6,10-12}, where the role of the Rashba¹³ as well as the Dresselhaus¹⁴ mechanisms for spin-orbit interaction in semiconductors have been investigated.

For two electron GaAs dots in particular, relaxation times on the millisecond timescale have been demonstrated experimentally^{6,11}, and the singlet-triplet energy-splitting, as well as relaxation rates, have been investigated in some detail for magnetic fields of up to a few Tesla. Previous theoretical efforts to model these studies have shown that the system seems to exhibit a smaller than expected Dresselhaus coefficient^{15,16} and that a cylindrical hard-wall potential reproduces the singlet-triplet energy-splitting more accurately than a harmonic oscillator potential¹⁷. In the present work, an elliptical cylinder potential is used to further study the realistic parameter range determining the energy splitting and relaxation rates of said system, motivated by the better energy-splitting agreement previously shown. Harmonic oscillator results are also produced using the

same methods and the differences in results due to potential shape are investigated.

This paper starts with a brief model- and implementation section describing what physical effects are included and how they are implemented. The electron wave-functions are represented in a B-spline basis¹⁸, allowing for an arbitrary potential shape. Magnetic effects, in the form of a tilted magnetic field, as well as spin-orbit (SO) effects are included in the one-body Hamiltonian. All the one-particle contributions to the Hamiltonian are used to create a basis which in turn is used to include the Coulomb interaction through the full configuration interaction (FCI) method. The two-electron states corresponding to the singlet ground state and first excited triplet states are extracted and used to calculate the phonon induced relaxation rate from Fermi's golden rule. Dot width, ellipticity and relative directions of the tilted magnetic field are varied to match the energy splitting profile from the experimental results.

Following the model and implementation section, the results show the calculated singlet-triplet energy splittings for different dot potentials and compared them to the experimental results by Meunier et al.⁶. This is followed by relaxation rates calculated for the same systems.

II. MODEL AND IMPLEMENTATION

A. Model

The two electron Hamiltonian describing the quantum dot can be expressed as

$$H = \sum_{i=1,2} h(\mathbf{r}_i) + \frac{e^2}{4\pi\epsilon_r\epsilon_0|\mathbf{r}_1 - \mathbf{r}_2|}, \quad (1)$$

where ϵ_r is the relative permittivity of the semiconductor material and $h(\mathbf{r}_i)$ is the one-particle Hamiltonian:

$$h(\mathbf{r}_i) = \frac{1}{2m^*} \hat{\Pi}^2 + g^* \mu_b \mathbf{B} \cdot \hat{\mathbf{S}} + V + h_{SO}. \quad (2)$$

Here $\hat{\mathbf{\Pi}}$ is the momentum operator, $\hat{\mathbf{S}}$ is the spin operator vector, V is the effective confinement potential and h_{SO} is the spin-orbit interaction. Bulk material properties are used for the electron effective mass m^* and gyromagnetic ration g^* . The magnetic field \mathbf{B} is tilted from the z-axis by an angle θ and azimuthally from the x-axis by ϕ , so that:

$$\mathbf{B} = B_0(\cos \phi \sin \theta, \sin \phi \sin \theta, \cos \theta), \quad (3)$$

and the kinetic energy operator can be expanded to:

$$\frac{1}{2m^*} \hat{\mathbf{\Pi}}^2 = -\frac{\hbar^2}{2m^*} \nabla^2 + \frac{e^2}{2m^*} A^2 + \frac{e}{2m^*} \mathbf{B} \cdot \hat{\mathbf{L}}. \quad (4)$$

Here we choose to study a QD restricted in the z-dimension, often orders of magnitude thinner than wide. We can divide the wave function as:

$$\Psi(\mathbf{r}) = \psi(x, y) \delta(z), \quad (5)$$

where the z-component is assumed to be in the shape of a Dirac delta function. This limits the vector potential to:

$$\mathbf{A} = \frac{B_0}{2} (-y \cos \theta, x \cos \theta, y \cos \phi \sin \theta - x \sin \phi \sin \theta), \quad (6)$$

and with these restrictions A^2 takes the form of an anisotropic harmonic oscillator potential in the xy-plane. The potential has an elliptical cross section and the minor axis lies along projection of the magnetic field in the xy-plane (i.e. in the ϕ direction),

$$A^2 = \frac{B_0}{4} [(x^2 + y^2) \cos^2 \theta + (y \sin \phi - x \cos \phi)^2 \sin^2 \theta]. \quad (7)$$

The angular momentum operator will also for this system be limited to $\hat{\mathbf{L}} = \hat{L}_z$ due to the restraints in the z-direction, leaving the angular momentum Zeeman term:

$$\frac{e}{2m^*} \mathbf{B} \cdot \hat{\mathbf{L}} = \frac{e}{2m^*} \cos \theta B_0 \hat{L}_z. \quad (8)$$

With \mathbf{B} placed along the z-axis, the electron spin states are eigenstates to the \hat{S}_z operator, leading to the Zeeman spin term shifting the states $|\pm 1/2\rangle$ by the energy:

$$\mp g^* \mu_b B_0 \hbar / 2. \quad (9)$$

With an inclined magnetic field the \hat{S}_z eigenstates will no longer be eigenstates to the Zeeman operator, instead the Zeeman spin term will couple the $|\pm 1/2\rangle$ states by:

$$g^* \mu_b \mathbf{B} \cdot \hat{\mathbf{S}} = g^* \mu_b B_0 \left(\cos \phi \sin \theta \hat{S}_x + \sin \phi \sin \theta \hat{S}_y + \cos \theta \hat{S}_z \right). \quad (10)$$

Note that this alone will not mix spins, but rather lead to spin up and down states (as defined by the direction of the magnetic field) that are linear combinations of the \hat{S}_z eigenstates according to:

$$|\uparrow\rangle = \cos(\theta/2)|+1/2\rangle - \sin(\theta/2)|-1/2\rangle, \quad (11)$$

and

$$|\downarrow\rangle = \sin(\theta/2)|+1/2\rangle + \cos(\theta/2)|-1/2\rangle, \quad (12)$$

with the same energy splitting as without any field inclination.

Spin mixing can occur through the spin-orbit Hamiltonian, $h_{SO} = H_R + H_{D1} + H_{D3}$, including the Rashba:

$$h_R = \frac{\alpha}{\hbar} (\hat{\pi}_x \hat{\sigma}_y - \hat{\pi}_y \hat{\sigma}_x), \quad (13)$$

the linear Dresselhaus:

$$h_{D1} = \frac{\gamma}{\hbar^3} (\hat{\pi}_z^2) (\hat{\pi}_y \hat{\sigma}_y - \hat{\pi}_x \hat{\sigma}_x), \quad (14)$$

and the cubic Dresselhaus:

$$h_{D3} = \frac{\gamma}{2\hbar^3} [(\hat{\pi}_x \hat{\pi}_y^2 \hat{\sigma}_x - \hat{\pi}_y \hat{\pi}_x^2 \hat{\sigma}_y) + (\hat{\pi}_x \hat{\pi}_y^2 \hat{\sigma}_x - \hat{\pi}_y \hat{\pi}_x^2 \hat{\sigma}_y)^\dagger]. \quad (15)$$

where α and γ are the Rashba and Dresselhaus coefficients, $\hat{\pi}_{x,y,z}$ are the momentum operators and $\hat{\sigma}_{x,y}$ are the Pauli spin matrices. The Rashba interaction conserves $m_l + m_s$ and linear Dresselhaus interaction conserves $m_l - m_s$. The cubic Dresselhaus operator couple states $|m_l, m_s\rangle$ according to the selection rules¹⁹:

$$\begin{aligned} |m_l, +1/2\rangle &\rightarrow |m_l - 1, -1/2\rangle, |m_l + 3, -1/2\rangle \\ |m_l, -1/2\rangle &\rightarrow |m_l + 1, +1/2\rangle, |m_l - 3, +1/2\rangle. \end{aligned} \quad (16)$$

Previous studies on similar systems have shown the Dresselhaus coupling to be the dominating spin-orbit interaction in this regime²⁰, with the cubic Dresselhaus term being of some significance²¹. The ratio between the Dresselhaus and Rashba coefficients may however still be of interest when studying an anisotropic QD under a tilted and rotated magnetic field¹², small Rashba coefficients have been tested and found not to change the results significantly and will not be investigated further in this paper.

In this work we focus on two effective confinement potentials; the two dimensional harmonic oscillator

$$V_{HO}(\mathbf{r}_i) = \frac{m^* \omega^2}{2} [(\delta x_i)^2 + (\frac{y_i}{\delta})^2], \quad (17)$$

where ω is the harmonic oscillator frequency and δ is the dot ellipticity; and the hard wall cylindrical potential

$$V_{HW}(\mathbf{r}_i) = \frac{m^* \omega^2}{2} \frac{[(\delta x_i)^2 + (\frac{y_i}{\delta})^2]^N}{r_0^{2(N-1)}}, \quad (18)$$

where N is a large integer, r_0 is the dot radius and ω is used to tune the dot to match the harmonic oscillator at r_0 . The hard wall potential is not a true step function at $|\mathbf{r}_i| = r_0$, but has a softness that is decreased with a high N value.

The phonon induced singlet-triplet relaxation rate is calculated from Fermi's golden rule:

$$\Gamma_i = \frac{V}{4\pi^2\hbar} \sum_{j=1}^3 \int d^3q |M_j(\mathbf{q})|^2 \left| \langle S | \hat{H}_{ph} | T_i \rangle \right|^2 \delta(\Delta E_{ST} - \hbar c_j q), \quad (19)$$

for triplet states T_{+1} , T_0 and T_{-1} . We include relaxation through three phonon effects⁹; deformation potential coupling

$$|M_1(\mathbf{q})|^2 = \frac{\hbar \Xi_d^2}{2\rho c_l V} |\mathbf{q}|, \quad (20)$$

longitudinal piezoelectric coupling

$$|M_2(\mathbf{q})|^2 = \frac{32\pi^2 \hbar e^2 h_{14}^2}{\epsilon_r^2 \rho c_l V} \frac{(3q_x q_y q_z)^2}{|\mathbf{q}^7|}, \quad (21)$$

and transversal piezoelectric coupling

$$|M_3(\mathbf{q})|^2 = \frac{32\pi^2 \hbar e^2 h_{14}^2}{\epsilon_r^2 \rho c_l V} \left(\frac{q_x^2 q_y^2 + q_y^2 q_z^2 + q_z^2 q_x^2}{|\mathbf{q}^5|} - \frac{(3q_x q_y q_z)^2}{|\mathbf{q}^7|} \right). \quad (22)$$

The last term is counted twice to account for two identical phonon modes²². Here ΔE_{ST} is the singlet-triplet energy splitting, $\mathbf{q} = (q_x, q_y, q_z)$ is the phonon momentum and the states couple through the $\hat{H}_{ph} = \sum_{i=1,2} e^{-i\mathbf{q}\cdot\mathbf{r}}$ operator. Linear dispersion is used so that the phonon momentum is matched to the energy splitting, $|\mathbf{q}| = q = \Delta E/(\hbar c_j)$, where c_j is the longitudinal speed of sound for $j = 1, 2$, and the transversal speed of sound for $j = 3$. V is the normalization volume that will be cancel out, Ξ_d is the deformation potential constant, ρ is the material mass density and h_{14} is the piezoelectric constant.

B. Implementation

The one-particle Schrödinger equation, Eq. (2), is solved through diagonalization of the Hamiltonian matrix within a numerical B-spline¹⁸ basis, where the polynomial basis allows for integration to machine precision through Gaussian quadrature. We note that the spin-orbit interaction is included already at this level and that spin-mixing thus is allowed within the full basis. It has earlier been shown in the literature^{23,24} that a large number of basis functions are needed in order to achieve convergence for the spin-orbit coupling even when only the lowest few many-body states are of interest.

Using a restricted set of the one-electron states obtained, all possible two-electron Slater determinants are constructed, and the full configuration interaction generalized eigenvalue equation is set up and solved through diagonalization of the two-particle Hamiltonian, matrix, c.f. Eq. 1. The selection of one-electron orbitals to include is made by choosing a maximum number of their

$\langle n_x + n_y \rangle$ quantity and monitoring the convergence in two-electron energy to within one percent. Here $n_{x/y}$ denote the quantum numbers for the one dimensional well or harmonic oscillator potential. The $\langle n_x + n_y \rangle$ quantity is quite constant for a specific state even in the presence of an elliptic potential and tilted magnetic field. In close proximity to any avoided crossings created e.g. by the spin-orbit interactions, $\langle n_x + n_y \rangle$ will change between the avoiding states.

We model a GaAs dot using bulk values for the effective mass, $m^* = 0.067m_e$, relative permittivity, $\epsilon_r = 14.4$ and effective gyromagnetic ratio $g^* = -0.44$. For the Dresselhaus parameter, we choose values of; $\gamma = 27.5 \text{ eV}\text{\AA}^3$, in accordance to previous experimental and theoretical results in GaAs,²⁵⁻²⁷; and $\gamma = 9 \text{ eV}\text{\AA}^3$, from previous system specific results,^{11,15,16}.

For the phonon transition calculations, a crystal density of $d = 5310 \text{ kg/m}^3$, deformation potential constant $\Xi_d = 6.7 \text{ eV}$, piezoelectric constant $h_{14} = 1.4 \text{ V/m}$ and sound velocities $c_L = 4720 \text{ m/s}$ longitudinal and $c_T = 3340 \text{ m/s}$ transversal are employed.

III. ONE-ELECTRON SPECTRUM

A study of the one-electron spectrum of the potentials will yield some important information on how the various parts of the one-electron Hamiltonian will effect the states. The key effect being the spin-orbit interaction and the avoided crossings appearing when it is included.

A. Harmonic Oscillator Confinement

The symmetric harmonic oscillator spectrum in Fig. 1 is familiar for a magnetic field perpendicular to the plane. The angular momentum Zeeman-splitting, linearly dependent on the B-field, dominates at low energies, but is overshadowed by the A^2 term at stronger fields, and at very high field strengths, Landau levels start forming. An important property of the harmonic oscillator is the equal-distance level spacing at zero magnetic field. A consequence of which is that the linear Zeeman splitting will create points where states bunch together and cross. One such point in Fig. 1 is around 1.26 T where states differing by multiples of $\Delta m_l = 3$ will cross.

By zooming in on the vicinity of the $m_l = +2, -1$, and -4 crossing, we see that the cubic Dresselhaus effect is creating an avoided crossing between the $|n, m_l, m_s\rangle = |0, +2, \downarrow\rangle$ and $|1, -1, \uparrow\rangle$ states as well as between the $|1, -1, \downarrow\rangle$ and $|0, -4, \uparrow\rangle$ states, as expected from the selection rules. In the vicinity of these crossings, the electron spins will be heavily mixed. Since all such $\Delta m_l = 3$ crossings are located at the same magnetic field strength, this should result in a "spin hot-spot" and many-electron states formed from these one-electron orbitals cannot be eigenstates to \hat{S}^2 any more.

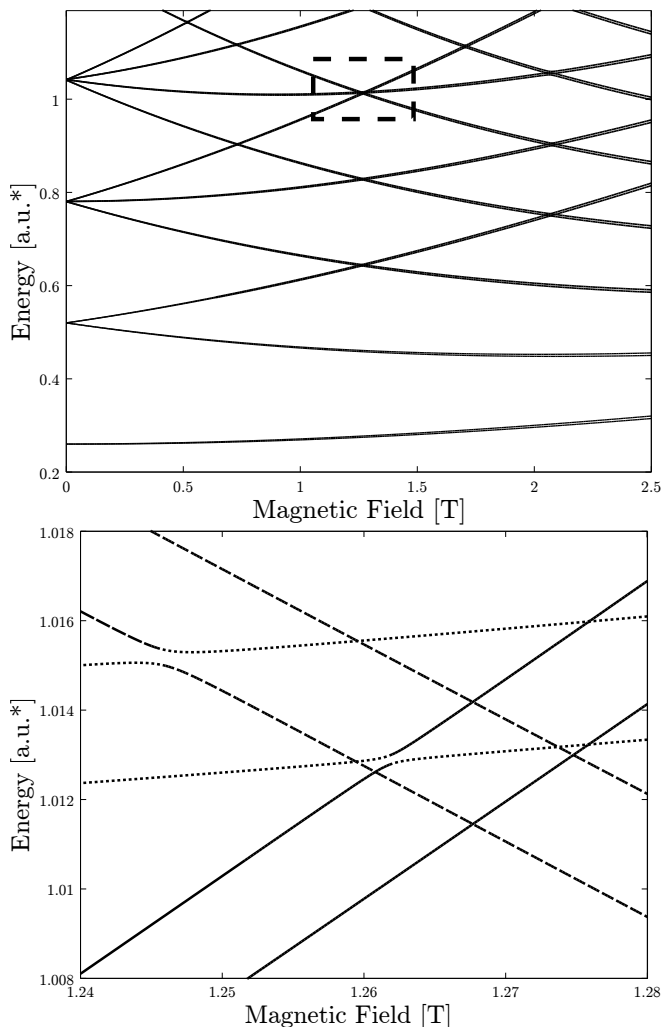


FIG. 1: Above: The one-electron spectrum of a symmetric harmonic oscillator, with $\hbar\omega = 2.96$ meV, as a function of the strength of a magnetic field perpendicular to the plane. Below: Enhancement of the dashed area in the figure above. Avoided crossings due to the cubic Dresselhaus effect seen between states $|0, +2, \downarrow\rangle$ (solid) \leftrightarrow $|1, -1, \uparrow\rangle$ (dotted) and $|1, -1, \downarrow\rangle$ (dotted) \leftrightarrow $|0, -4, \uparrow\rangle$ (dashed).

The case of the elliptic harmonic oscillator with a tilted magnetic field, Fig. 2, has at a first glance a similar spectrum as the symmetric case. Noticeable differences being an overall scaling since the magnetic z -component is dampened by a factor $\cos\theta$; and the splitting of states at low field strength due to the ellipticity. Since the angular momentum operator, \hat{L}_z , is independent of r , it commutes with the circular symmetric harmonic oscillator potential, and it is possible to choose eigenfunctions that are simultaneously eigenfunctions to the Hamiltonian and to \hat{L}_z . An elliptic potential, however, does not commute with \hat{L}_z . No common eigenfunctions can then be found and the elliptical states at low magnetic field strengths are highly mixed in m_l , and as a consequence they respond weakly to the Zeeman effect. Once the

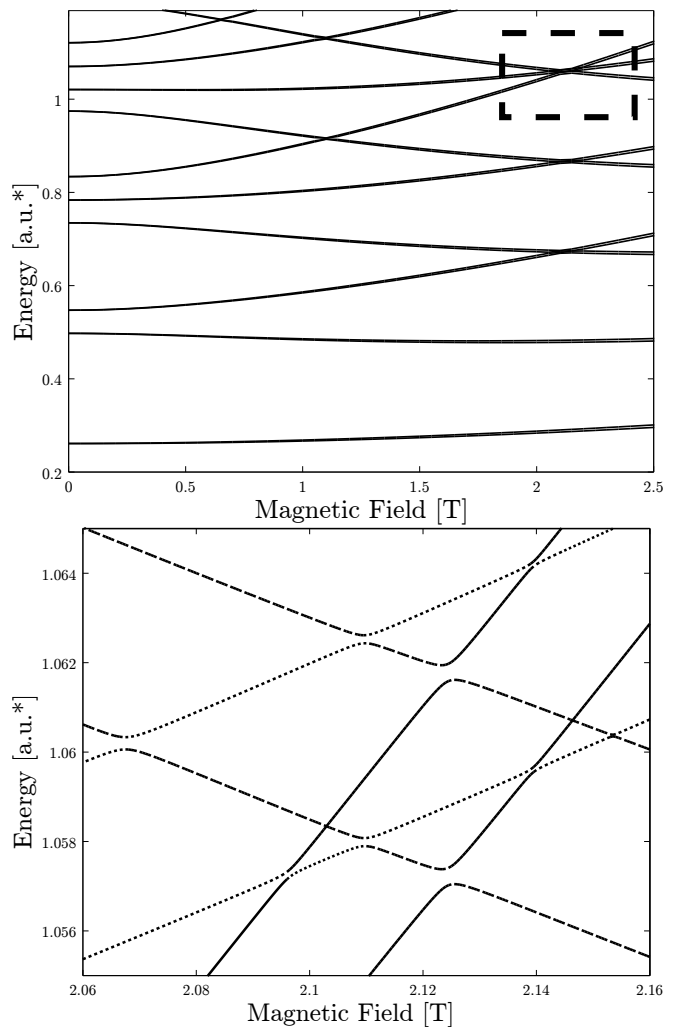


FIG. 2: Above: The one-electron spectrum of an elliptic harmonic oscillator, with $\hbar\omega = 2.96$ meV and $\delta = 1.1$, as a function of the strength of a tilted magnetic field, with angles $\theta = 55^\circ$ and $\phi = 90^\circ$. Below: Enhancement of the dashed area in the figure above. Avoided crossings between many states due to the spin states not being pure \hat{S}_z eigenstates. Line styles as in figure 1.

magnetic field strength is strong enough to dominate over the potential, states can once again be approximately described by their m_l quantum number, and will start to split linearly with $\cos\theta B_0$.

The crossing points seen in the symmetrical harmonic oscillator will however persist, but at scaled field strengths, since these are a result of the linear Zeeman splitting that still dominates in this region. The crossing at 1.26 T in Fig. 1, has for instance been shifted to 2.11 T in Fig. 2.

A more detailed investigation of the state crossings reveals that many more avoided crossings are created by the spin-orbit interaction in the elliptic case. Since the spin states are a linear combination of the \hat{S}_z eigenstates, they both will couple to states of $\Delta m_l = 3$. Also second

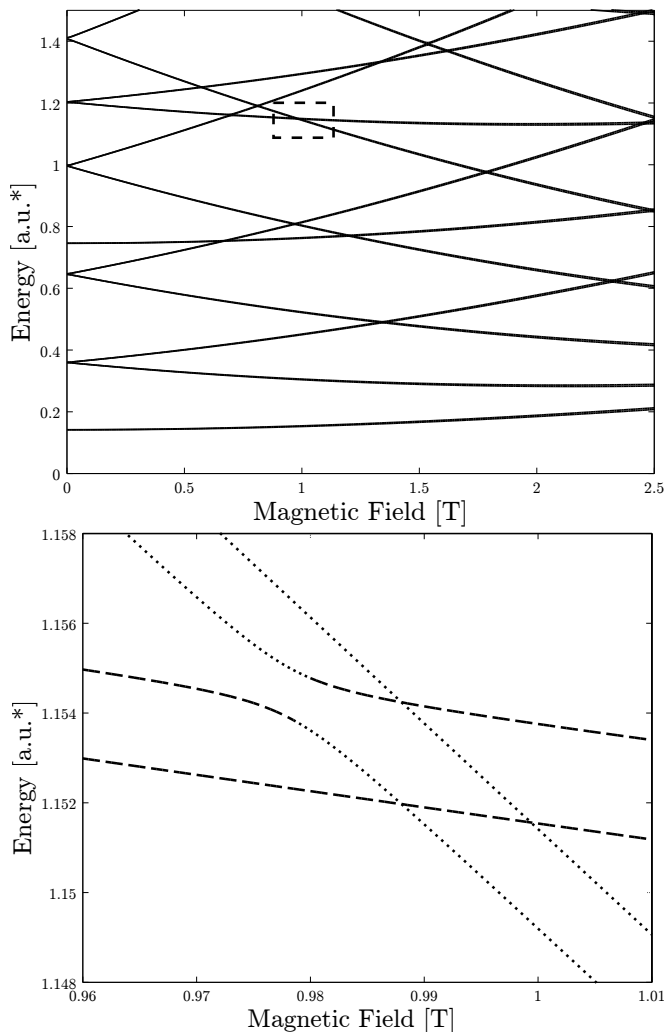


FIG. 3: Above: The one-electron spectrum of a circular well, with $r_0 = 44$ nm, as a function of the strength of a magnetic field perpendicular to the plane. Below: Enhancement of the dashed area in the figure above. Avoided crossings due to the cubic Dresselhaus effect seen between the $|1, -1, \downarrow\rangle$ (dotted) and $|0, -4, \uparrow\rangle$ (dashed) states.

order effects appear, coupling states of $\Delta m_l = 6$. This will result in heavy spin mixing occurring over a broader magnetic field range, resulting in a larger spin hot-spot than in the case with a circular symmetric confinement potential.

B. Cylinder Well Confinement

Fig. 3 shows the one-electron energy spectra for a circular well with a magnetic field perpendicular to the plane. The one-electron state energies at zero magnetic field will differ between the circular well and harmonic oscillator. Since the electrons in the well are strictly confined within the radius of the dot, states with higher radial quantum numbers will have higher energies than

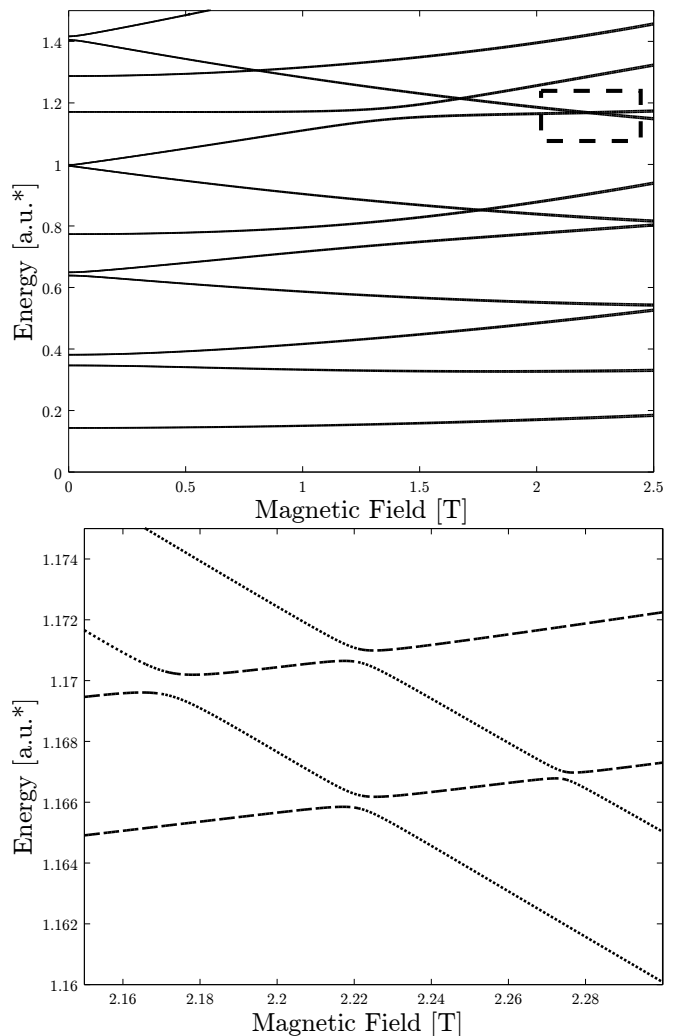


FIG. 4: Above: The one-electron spectrum of a elliptic well, with $r_0 = 44$ nm and $\delta = 1.05$, as a function of the strength of a tilted magnetic field with angles $\theta = 60^\circ$ and $\phi = 90^\circ$. Below: Enhancement of the dashed area in the figure above. Avoided crossings between several states due to the spin states not being pure \hat{S}_z eigenstates. Linestyles as in Fig. 3

their harmonic oscillator counterparts. The resulting energy level structure, and degeneracies will therefore differ.

The angular components of the circular quantum well eigenstates are equivalent to the harmonic oscillator polar angular components, and are hence eigenfunctions to the angular momentum operator. This results in a Zeeman splitting for the circular well states, much in the same manner as for the harmonic oscillator, until the A^2 -term once again starts to dominate, and Landau levels begin forming.

An important consequence of not having equidistant energy levels at zero magnetic field is the lack of high degeneracy at certain field strengths, as those found in the harmonic oscillator. This should reduce the effect of spin hot-spots, and instead spread out the spin mixed states over the entire spectra. In the zoomed in part of Fig. 3,

an avoided crossing due to the cubic Dresselhaus interaction can be seen between the $|1, -1, \downarrow\rangle$ and $|0, -4, \uparrow\rangle$ states.

The ellipticity and tilted field added to Fig. 4 produces similar results to those found in the elliptic harmonic oscillator. The shift due to the scaled z-component of the magnetic field will not behave quite as linearly though, and some state crossings will disappear or be shifted far from the magnetic area of interest.

As in the harmonic oscillator case, the spin states, being linear combinations of the \hat{S}_z eigenstates, will form avoided crossings with more states for a tilted magnetic field, as compared to the case with a field perpendicular to the xy -plane.

IV. TWO-ELECTRON RESULTS

The four lowest two-particle states obtained by diagonalization of the two-particle Hamiltonian matrix, c.f. Eq. 1, are: a singlet state, which is the ground state for modest B-fields, and the Zeeman-split triplet states, with $M_S = -1, 0, 1$. The position of the three latter with respect to the ground states is shown as a function of magnetic field in Fig. 5.

In the following we want to compare our calculations to the experiment by Meunier et al.⁶, and the first question is which of the states that were really addressed there. They claim to populate all three triplet states, and that the measurements are done on an average over these. We doubt that this is the case and that the most likely triplet state to populate should be the lowest energy spin polarized state. The experiment starts with a single electron trapped in the dot, a second electron is then allowed to tunnel into the dot, creating either a singlet or triplet state. An electron is then allowed to tunnel out and a change in current is observed with a quantum point contact. Based on tunneling rates the two-electron state is said to be determined. With the first electron in a definite state⁶, e.g. the single particle ground state (in the presence of the magnetic field), $|g, \uparrow\rangle$, the second electron can populate the $|g, \downarrow\rangle$ orbital or the $|e, \uparrow\rangle$ orbital forming the singlet ground state or the spin-polarized triplet state, $T_+ = \{|g, \uparrow\rangle|e, \uparrow\rangle\}$, respectively, where T_+ is labeled by its dominating configuration. In this case the $T_- = \{|g, \downarrow\rangle|e, \downarrow\rangle\}$ configuration cannot be reached at all. Since the true states are better described as a superposition of configurations they can of course be entered through other configurations, but this is expected to be a less efficient path.

The T_0 state, finally, should be dominated by a linear combination of the different possibilities there are to form a $M_S = 0$ state from the two lowest orbitals; $T_0 = \frac{1}{\sqrt{2}} \{|g, \uparrow\rangle|e, \downarrow\rangle + |g, \downarrow\rangle|e, \uparrow\rangle\}$. Starting with one electron in a definite spin-state we can only enter this state through one of the configurations and the state will consequently be less efficiently populated. In addition we should expect to form the corresponding excited singlet

state in the case when it is energetically allowed. This understanding is further supported by later experiments on similar systems²⁸, where only one of the polarized triplets and an unpolarized state is found to be created in addition to the lowest energy singlet state.

Due to the uncertainty regarding the individual population of the three triplet states, we have chosen to investigate all three states separately rather than averaging over them.

A. Singlet-Triplet Splitting

The experimental results used for comparison¹¹ come from a system with few parameter details. The inclination of the magnetic field, measured through Shubnikov-Haas oscillations, is $68 \pm 5^\circ$, with an unknown azimuthal angle. From the singlet-triplet energy splitting measured and the constant splitting at low magnetic fields, we estimate the harmonic oscillator strength to be around $\hbar\omega = 3$ meV with an ellipticity $\delta = 1.1$, or a well radius of $r_0 = 44$ nm with an ellipticity $\delta = 1.05$. These are rough estimates, but lead to energy splittings as those seen in Fig. 5, which are in good agreement with the experiment.

If other parameters are used the energy splitting curve will change, leading to a less good agreement. For example: First, if the dot is widened, i.e. the radius is increased or the oscillator strength is decreased, the Coulomb repulsion between the electrons will decrease. Since the ground state singlet has a larger correlation energy than the excited triplet, it will be effected more by the potential change, resulting in a translation of the energy splitting curve to a lower energy, which will worsen the comparison with the experimental data.

Second, the ellipticity will both affect the energy splitting at zero field, and at what field strength the magnetic field starts to decrease the splitting. As seen in Fig. 2 and 4, the first excited one-electron state shifts down in energy when an ellipticity is introduced. This reduces the total energy of the triplet state since it is dominated by a configuration where one of the two electrons occupies this orbital. The splitting plateau lasts until the one-electron Zeeman term is large enough to start shifting the energies as discussed in the previous section. The ellipticity $\delta = 1.1$ in the harmonic case, and $\delta = 1.05$ for the well, were found to give the best agreement with the experimental data.

Third, the dominating magnetic effect in the investigated field range comes from the linear Zeeman splitting which is directly scaled by the inclination angle with a factor of $\cos\theta$. Unsurprisingly the inclination angle will then also affect the singlet-triplet splitting, where a large angle results in a weaker magnetic dependence. The inclination angle is thus rather strictly limited to the 55° and 60° found here for the two confinement potentials. The in-plane, azimuthal angle will determine the direction of the elliptic A^2 potential, and will shift m_l states some-

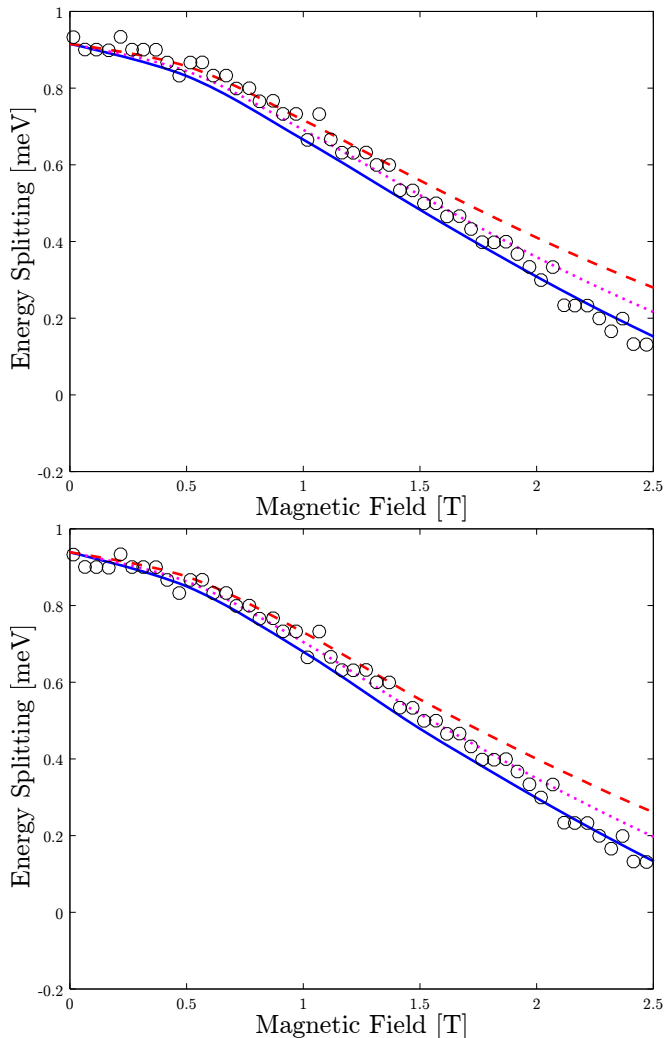


FIG. 5: Above: The singlet-triplet splitting of an elliptic harmonic oscillator, with $\hbar\omega = 2.96$ meV and $\delta = 1.1$, as a function of the strength of a tilted magnetic field, with angles $\theta = 55^\circ$ and $\phi = 90^\circ$. The three triplet states are the first excited $M_S = -1$ (solid), $M_S = 0$ (dotted) and $M_S = +1$ (dashed) states. The circles show the experimental results¹¹. Below: The singlet-triplet splitting for an elliptic well, with $r_0 = 44$ nm and $\delta = 1.05$, as a function of the strength of a titled magnetic field with angles $\theta = 60^\circ$ and $\phi = 90^\circ$.

what. It will however be a small effect compared to the effect from the Zeeman splitting when operating within the field range studied here. We find thus, as was also concluded previously¹⁷, that the splitting in the cylindrical well potential matches the experimentally measured inclination angle better than the harmonic, case although it is still somewhat on the low side.

As a final remark regarding the magnetic field inclination angle, we note that both the investigated effective potentials are two dimensional, there might in addition be some effects from the confinement in the z-dimension that could better the agreement for both potentials. In-

clusion of electron motion in the z-direction will allow the tilted field to couple not only to the in plane momentum, but also to the perpendicular one, possibly leading to a smaller singlet-triplet splitting, but has not been investigated further here.

B. Relaxation

We now study the relaxation rate as a function of the singlet-triplet splitting from the previous section.

If only the dominating configurations are considered for the triplet states, one would expect drastically different relaxation times²⁹ for T_{-1}, T_0, T_1 , however the combination of configuration interaction and spin-orbit mixing has been shown to give much less pronounced differences for T_{-1} and T_1 ²⁴. Our results are slightly different than what has been found in other studies. With only the linear Dresselhaus interaction present we find, in agreement with most of the literature^{30,31}, that the T_0 state is much more long-lived than the other two, but when also the cubic Dresselhaus is included this is no longer the case. We note that Meunier et al.¹¹ mention that they do not observe any slowly relaxing triplet component in the experiment. More recent experiments²⁸, also demonstrate shorter than expected T_0 lifetimes. One possibility is that this is due to a less efficient population of T_0 as discussed above, or that its relaxation is indeed faster than often believed. Below we discuss the relaxation for the the two different confinement potentials in more detail.

1. Harmonic Oscillator Confinement

In the case when only the linear Dresselhaus interaction is included, Fig. 6, we find a relaxation maximum around 0.25 meV where the electronic state width matches the wavelength of the phonon. We are not able to reproduce the relaxation rate plateau found at weak fields in the experiment, even though this type of structure is found in the energy splitting. Possibly some other relaxation processes dominate at these low field strengths. The relaxation rates from the spin polarized triplet state, T_{+1} and T_{-1} , are fairly equal in respect to the energy splitting dependence, with the unpolarized T_0 state mostly exhibiting a significantly smaller rate, as expected^{30,31}. Some structures in the curves seem dependent on the magnetic field rather than the phonon energy, namely the dip in rate for the T_{+1} and T_{-1} around 0.65 meV and the peaks in T_{+1} and T_0 around 0.3 meV. These points correspond to magnetic field strengths of 1.1 and 2.1 T, where we also find the crossings of many of the one-electron basis states discussed in Sec. III A.

For the calculations where the cubic Dresselhaus has been included, the parameter γ has been tuned down so that the peak in relaxation roughly matches the experimental data. The avoided crossings become even more obvious when the cubic Dresselhaus term is included,

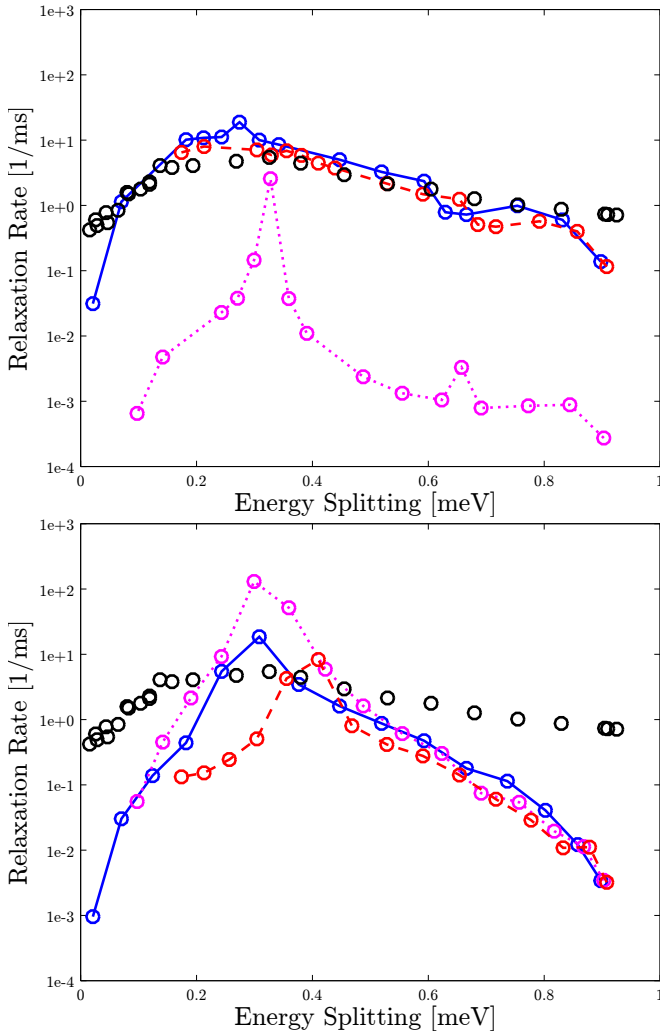


FIG. 6: The relaxation rate as a function of the singlet-triplet energy splitting for an elliptic harmonic oscillator, with $\hbar\omega = 2.96$ meV and $\delta = 1.1$, in a tilted magnetic field, with angles $\theta = 55^\circ$ and $\phi = 90^\circ$. The three triplet states are the first excited $M_S = -1$ (solid), $M_S = 0$ (dotted) and $M_S = +1$ (dashed) states. The circles without interconnecting lines show the experimental results¹¹. Above: The relaxation rate for $\gamma = 27$ $\text{ev}\text{\AA}^3$, $\hbar\omega_z = 11.85$ meV and no cubic Dresselhaus interaction. Below: The rate for $\gamma = 9$ $\text{ev}\text{\AA}^3$, $\hbar\omega_z = 11.85$ meV with cubic Dresselhaus interaction.

where the crossing point of basis states of $\Delta m_l = 3$ becomes a spin hot-spot with a relaxation rate that does not match anything found in the experimental data. Since the relation between the linear and cubic Dresselhaus terms is governed by the z-thickness through $\langle \pi_z^2 \rangle$, a thinner dot should have a increased rate due to a larger linear contribution³². If large enough it should be able to overshadow the cubic contribution. A thickness corresponding to an oscillator strength of $\hbar\omega_z = 11.85$ meV is used here in accordance to previous studies^{11,15,16}. With this value, the cubic effect seems indeed to be a substantial effect that should be noticeable in the rates measured.

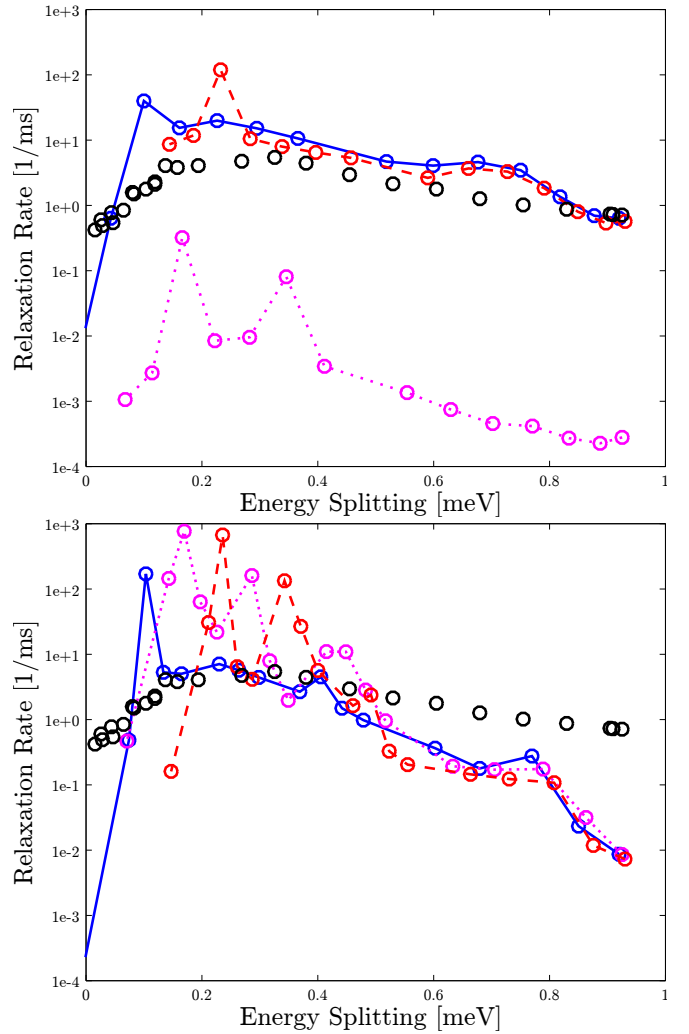


FIG. 7: The relaxation rate as a function of the singlet-triplet energy splitting for an elliptic cylindrical well, with $r_0 = 44$ nm and $\delta = 1.05$, in a tilted magnetic field, with angles $\theta = 60^\circ$ and $\phi = 90^\circ$. The three triplet states are the first excited $M_S = -1$ (solid), $M_S = 0$ (dotted) and $M_S = +1$ (dashed) states. The circles without interconnecting lines show the experimental results¹¹. Above: The relaxation rate for $\gamma = 27$ $\text{ev}\text{\AA}^3$, $\hbar\omega_z = 11.85$ meV and no cubic Dresselhaus interaction. Below: The rate for $\gamma = 9$ $\text{ev}\text{\AA}^3$, $\hbar\omega_z = 11.85$ meV with cubic Dresselhaus interaction.

An increased strength of the z-confinement, which should tune down the relative importance of the cubic effect, needs however to be compensated by a reduced γ . In this case it should be possible to find a better fit to the experimental results, however at a much lower Dresselhaus coefficient than expected.

In the previous section, to produce the singlet-triplet energy splitting from the experimental data, a smaller than expected field inclination angle was required. This shifted the $\Delta m_l = 3$ harmonic crossing point from 1.25 T in the case of a perpendicular magnetic field, to roughly 2.1 T with an inclination of $\theta = 55^\circ$. With the ex-

perimentally measured inclination angle of $\theta = 68^\circ$, this crossing should be found around 3.3 T, beyond the investigated magnetic field range. It is possible that some three dimensional, or other, effect not included can change the results to better match the measurements, and through that remove the issue with the cubic Dresselhaus effect spin hot-spot.

2. Cylinder Well Confinement

The relaxation rate in the case of the cylinder well with only linear Dresselhaus interaction is similar to the harmonic case, as seen in Fig. 7. The peaks are due to avoided crossings in the one-electron spectrum, however differently placed than in the harmonic oscillator. Small structures in the experimental data may be indicative of the underlying one-electron avoided crossings, these are however not as obvious as in our calculations. The overall rate is higher than in the harmonic case when only including the linear interaction, indicating an even smaller Dresselhaus coefficient.

When the cubic effect is included, the avoided crossing points become more prominent since the total interaction is increased. More and larger peaks are present, especially for the T_0 and T_{+1} states, to the extent that only the T_{-1} state seems to match the experimental data. The main difference to the harmonic oscillator is the lack of a large surge in relaxation around the point of multiple crossings, which does not exist in the cylindrical well.

The difference in relaxation rate between low and high energy splittings is far larger than in the experimental data, however with a wider and flatter peak than in the harmonic oscillator case. Altering the modeled thickness of the dot and adjusting the Dresselhaus coefficient thereafter can possibly improve this.

V. CONCLUSION

A good fit to the experimental singlet-triplet splittings calculated for the two effective potentials produce similar results for slightly different inclination angles for the two

studied confinement potentials. The hard wall cylindrical well shows better agreement with the nominal value of the experiment than the harmonic oscillator potential, likely due to the stricter electron confinement in the well potential. The still existing discrepancy between the calculated and measured inclination angle can possibly be explained by the lacking finite z-potential in the calculations.

Good agreement for the relaxation rate is achieved when only the linear Dresselhaus term is included in the computations, although a Dresselhaus coefficient of $\gamma = 27 \text{ eV}\text{\AA}^3$ produces somewhat larger relaxation rates than the experimental data, but it can be tuned down slightly for better agreement. Some magnetic field dependent features can be seen in the relaxation curves, where the avoided crossings in the one-particle spectrum occur. These peaks are thin and fairly weak, and may be hard to detect in the experimental results.

A main finding in the present study is that inclusion of the cubic term significantly changes the results. For the harmonic confinement the results are clearly at odds with the experiment. For hard wall confinement the spin polarized T_{-1} still shows some resemblance to the experiment while the other states are too affected by the avoided spin crossings in the one-electron spectra, creating a large peak in relaxation around these points. The qualitative differences between the two potential shapes indicate that the choice of potential may be very important in modeling few electron quantum dots. Altering the z-confinement may reduce the influence of the cubic term, but will need to be compensated with a smaller Dresselhaus coefficient.

Acknowledgments

Financial support by the Swedish Research Council (VR), Grant No. 2016-03789, is gratefully acknowledged. We would also like to thank Professor Jan Petter Hansen and Professor Esa Räsänen for providing data and helpful discussions.

¹ Igor Žutić, Jaroslav Fabian, and S. Das Sarma. Spintronics: Fundamentals and applications. *Rev. Mod. Phys.*, 76:323–410, Apr 2004.

² Daniel Loss and David P. DiVincenzo. Quantum computation with quantum dots. *Phys. Rev. A*, 57:120–126, Jan 1998.

³ Miro Kroutvar, Yann Ducommun, Dominik Heiss, Max Bichler, Dieter Schuh, Gerhard Abstreiter, and Jonathan J. Finley. Optically programmable electron spin memory using semiconductor quantum dots. *Nature*, 432(7013):81–84, Nov 2004.

⁴ Toshimasa Fujisawa, David Guy Austing, Yasuhiro

Tokura, Yoshiro Hirayama, and Seigo Tarucha. Allowed and forbidden transitions in artificial hydrogen and helium atoms. *Nature*, 419(6904):278–281, Sep 2002.

⁵ J. M. Elzerman, R. Hanson, L. H. Willems van Beveren, B. Witkamp, L. M. K. Vandersypen, and L. P. Kouwenhoven. Single-shot read-out of an individual electron spin in a quantum dot. *Nature*, 430(6998):431–435, Jul 2004.

⁶ R. Hanson, L. H. Willems van Beveren, I. T. Vink, J. M. Elzerman, W. J. M. Naber, F. H. L. Koppens, L. P. Kouwenhoven, and L. M. K. Vandersypen. Single-shot readout of electron spin states in a quantum dot using spin-dependent tunnel rates. *Phys. Rev. Lett.*, 94:196802,

- May 2005.
- ⁷ S. A. Sørngrd, M. Førre, and J. P. Hansen. Angular resolved phonon emission from excited quantum dots. *New J. Phys.*, 14:013035, Jan 2012.
 - ⁸ Sanjay Prabhakar, Roderick Melnik, and Luis L. Bonilla. Electrical control of phonon-mediated spin relaxation rate in semiconductor quantum dots: Rashba versus dresselhaus spin-orbit coupling. *Phys. Rev. B*, 87:235202, Jun 2013.
 - ⁹ Juan I. Climente, Andrea Bertoni, Guido Goldoni, and Elisa Molinari. Phonon-induced electron relaxation in weakly confined single and coupled quantum dots. *Phys. Rev. B*, 74:035313, Jul 2006.
 - ¹⁰ M. Prada, R. H. Blick, and R. Joynt. Singlet-triplet relaxation in two-electron silicon quantum dots. *Phys. Rev. B*, 77:115438, Mar 2008.
 - ¹¹ T. Meunier, I. T. Vink, L. H. Willems van Beveren, K.-J. Tielrooij, R. Hanson, F. H. L. Koppens, H. P. Tranitz, W. Wegscheider, L. P. Kouwenhoven, and L. M. K. Vandersypen. Experimental signature of phonon-mediated spin relaxation in a two-electron quantum dot. *Phys. Rev. Lett.*, 98:126601, Mar 2007.
 - ¹² P. Scarlino, E. Kawakami, P. Stano, M. Shafiei, C. Reichl, W. Wegscheider, and L. M. K. Vandersypen. Spin-relaxation anisotropy in a gaas quantum dot. *Phys. Rev. Lett.*, 113:256802, Dec 2014.
 - ¹³ F.V. and Rashba E.I Kusmartsev. Properties of a 2d electron gas with lifted spectral degeneracy. *Sov. Phys. JETP*, 59:668–675, 1984.
 - ¹⁴ G. Dresselhaus. Spin-orbit coupling effects in zinc blende structures. *Phys. Rev.*, 100:580–586, Oct 1955.
 - ¹⁵ J. P. Hansen, S. A. Sørngård, M. Førre, and E. Räsänen. Quantitative modeling of spin relaxation in quantum dots. *Phys. Rev. B*, 85:035326, Jan 2012.
 - ¹⁶ Juan I. Climente, Andrea Bertoni, Guido Goldoni, Massimo Rontani, and Elisa Molinari. Effect of electron-electron interaction on the phonon-mediated spin relaxation in quantum dots. *Phys. Rev. B*, 76:085305, Aug 2007.
 - ¹⁷ T. Frostad, J. P. Hansen, C. J. Wesslén, E. Lindroth, and E. Räsänen. Two-electron quantum dot in tilted magnetic fields: Sensitivity to the confinement model. *The European Physical Journal B*, 86(10):1–6, 2013.
 - ¹⁸ Carl deBoor. *A Practical Guide to Splines*. Springer-Verlag, New York, 1978.
 - ¹⁹ Peter Stano and Jaroslav Fabian. Spin-orbit effects in single-electron states in coupled quantum dots. *Phys. Rev. B*, 72:155410, Oct 2005.
 - ²⁰ Alexander V. Khaetskii and Yuli V. Nazarov. Spin-flip transitions between zeeman sublevels in semiconductor quantum dots. *Phys. Rev. B*, 64:125316, Sep 2001.
 - ²¹ Jacob J. Krich and Bertrand I. Halperin. Cubic dresselhaus spin-orbit coupling in 2d electron quantum dots. *Phys. Rev. Lett.*, 98:226802, May 2007.
 - ²² J. David Zook. Piezoelectric scattering in semiconductors. *Phys. Rev.*, 136:A869–A878, Nov 1964.
 - ²³ J. L. Cheng, M. W. Wu, and C. Lü. Spin relaxation in gaas quantum dots. *Phys. Rev. B*, 69:115318, Mar 2004.
 - ²⁴ K. Shen and M. W. Wu. Triplet-singlet relaxation in semiconductor single and double quantum dots. *Phys. Rev. B*, 76:235313, Dec 2007.
 - ²⁵ J. B. Miller, D. M. Zumbühl, C. M. Marcus, Y. B. Lyanda-Geller, D. Goldhaber-Gordon, K. Campman, and A. C. Gossard. Gate-controlled spin-orbit quantum interference effects in lateral transport. *Phys. Rev. Lett.*, 90:076807, Feb 2003.
 - ²⁶ Shanhui Fan, Pierre R. Villeneuve, J. D. Joannopoulos, M. J. Khan, C. Manolatou, and H. A. Haus. Theoretical analysis of channel drop tunneling processes. *Phys. Rev. B*, 59:15882–15892, Jun 1999.
 - ²⁷ W. Knap, C. Skierbiszewski, A. Zduniak, E. Litwin-Staszewska, D. Bertho, F. Kobbi, J. L. Robert, G. E. Pikus, F. G. Pikus, S. V. Iordanskii, V. Mosser, K. Zekentes, and Yu. B. Lyanda-Geller. Weak antilocalization and spin precession in quantum wells. *Phys. Rev. B*, 53:3912–3924, Feb 1996.
 - ²⁸ H. Kiyama, T. Nakajima, S. Teraoka, A. Oiwa, and S. Tarucha. Single-shot ternary readout of two-electron spin states in a quantum dot using spin filtering by quantum hall edge states. *Phys. Rev. Lett.*, 117:236802, Nov 2016.
 - ²⁹ Juan I. Climente, Andrea Bertoni, Guido Goldoni, Massimo Rontani, and Elisa Molinari. Magnetic field dependence of triplet-singlet relaxation in quantum dots with spin-orbit coupling. *Phys. Rev. B*, 75:081303, Feb 2007.
 - ³⁰ Vitaly N. Golovach, Alexander Khaetskii, and Daniel Loss. Spin relaxation at the singlet-triplet crossing in a quantum dot. *Phys. Rev. B*, 77:045328, Jan 2008.
 - ³¹ Marian Florescu and Pawel Hawrylak. Spin relaxation in lateral quantum dots: Effects of spin-orbit interaction. *Phys. Rev. B*, 73:045304, Jan 2006.
 - ³² Josep Planelles, Juan I. Climente, and Carlos Segarra. Electron spin relaxation in 3d quantum dots: Geometrical suppression of dresselhaus and rashba spinorbit interaction. *The Journal of Physical Chemistry C*, 116(47):25143–25146, 2012.